Single-sensor RF Emitter Localization based on Multipath Exploitation

Alan C. O'Connor, *Member, IEEE,* Pawan Setlur, *Member, IEEE,* and Natasha Devroye, *Member, IEEE*

***Abstract*—This paper considers the problem of passive localization of a RF emitter by exploiting the multipath interaction of the signal with the environment, as occurs in urban settings. The feasibility of localizing using times-of-arrival (TOA) of multipath components is examined. The primary contribution is a method to correctly associate measured TOA with scatterering surfaces. Simulations are used to test the effects of scene geometry, clutter, and surface roughness on localization performance. *Index Terms*—source localization, multipath exploitation, urban sensing**

I. Introduction

Passive RF emitter localization is important in intelligence, surveillance and reconnaissance (ISR), as well as public safety operations. In urban or indoor settings, RF emissions are observed after interactions with the complex reflecting environment. Typically, multipath is considered an adverse condition; however, , exploiting the effects of multipath interaction can enable a new capability: RF emitter localization using only a single sensor.

The concept used to exploit multipath propagation effects in this paper requires some knowledge of the scattering environment. The waveform received at the single physical receiver is processed to obtain a number of virtual time-of-arrival (TOA) measurements at a constellation of virtual receivers. The positions of these virtual receivers are related to that of the single physical receiver through simple principles of ray optics. Localization is then performed as in the Global Positioning System (GPS), with multipath providing the needed spatial diversity.

A single-platform, single-antenna localization system has several advantages compared with a multi-platform system, or systems utilizing a single platform equipped with an antenna array. Multi-platform localization systems based on TOA-measurements require precise synchronization. Methods that measure frequency differences between receivers (differential Doppler) also require extremely accurate and stable local oscillators at the physically distributed receivers, as has been noted by [8], [1]. In contrast, a single sensor system like the one studied in this paper does not require any synchronization procedures, because all signals used for localization are obtained through the same antenna and A/D conversion chain. A second difficulty in a multi-platform system is the need for raw received waveform data to be transmitted between platforms. Eliminating the need for communication between multiple sensor platforms is particularly beneficial for systems that must operate covertly. Compared with a multi-antenna system, solving the localization problem using a single antenna system allows for a simpler, cost-effective, and physically smaller hardware implementation. These benefits make multipath exploitation an attractive localization approach for small UAVs operating in complex urban environments.

On the other hand, the difficulties involved in a single-sensor localization scheme are manifold. These difficulties are considered and addressed in this paper, and the scope of applicability of the proposed approach is described. First, as in multipath exploitation radar [17], [19], [25], the scattering environment must be known with some precision. A sufficient number of multipath components that correspond to known scattering surfaces must be detected, . Second, the measured TOAs must each be associated with a propagation path. In addition, any TOA that results from unmodeled scatterers must be identified as clutter and excluded from the localization algorithm.

A. Literature Review

There is an extensive literature on localizing RF emitters based on measurements collected at spatially distributed sensors. In some cases, these measure times-of-arrival (TOA) or time-differences-of-arrival (TDOA) [20], [33], frequency-differences-of-arrival (FDOA) also known as differential Doppler [1], [33], or angle-of-arrival (AOA) [11]. Other works have considered more complicated sensors that can make multiple measurement types. Specifically, TOA+FOA measurements were combined in [8], [15], [29], TOA+AOA in [23], and FOA+AOA in [5]. As a final example, in [4], a single mobile receiver measured TOA and FOA at multiple points of a trajectory to obtain the necessary spatial diversity to localize an emitter. The approach in this paper is most similar to the TOA systems; the novelty is to replace the spatial diversity from multiple sensors by using multipath exploitation.

Several past works have considered localization of emitters embedded in a multipath environment. In most of these works the focus is to mitigate the adverse effects of unmodeled non-line-of-sight (NLOS) propagation when one of the localization techniques described previously are adapted to a multipath environment. In particular, [7] developed a weighting scheme to mitigate effects of NLOS in TDOA localization, and [6] gave an algorithm to identify those receivers that had gotten the emitted signal along an NLOS path in order to exclude those TOA measurements from the localization algorithm. More recently, attention has turned to exploiting multipath

A. O'Connor was supported by a National Research Council Postdoctoral Fellowship held at the Air Force Research Laboratory, Sensors Directorate. P. Setlur and N. Devroye were partially supported by AFOSR under award FA9550-10-1-0239.

scattering to obtain a kind of virtual spatial diversity with a reduced number of physical sensors.

In [13], a model to predict multipath TOAs was developed; the local stability of the TOAs with respect to receiver motion could be used to maintain the performance of a localization system based on multiple RF sources when occlusions blocked LOS propagation paths. Seow and Tan [23] developed a specialized localization method for sensors capable of measuring both time- and angle-of-arrival in a scattering environment where all surfaces are horizontal or vertical planes.

The method of virtual receivers, which we use, has been previously used to understand and model the effect of multipath propagation of signals both in the context of RF emitter localization [20], [21], [27] and multipath-exploitation radar [12], [19], [25]. The paper [27] considered multipath in the context of multiple mobile stations cooperating to determine their absolute positions using signals emitted by a single base-station. The primary contribution was to determine the variance bounds on the position accuracy in the presence of multipath. Exploiting multipath as is done here was never their objective.

The paper [20] considered how single-bounce multipath time-of-arrival information could be used to enhance the accuracy with which an RF emitter could be localized by a system of spatially separated receivers. They assumed specular multipath from a single linear scattering surface in 2D space. Extending the method in [20] to a more complex environment including multiple scattering surfaces and clutter greatly increases the difficulty of the problem. In particular, neither [27] nor [20] addressed the problem of associating measured multipath TOAs to scatterers, which is a primary focus of the present contribution.

Finally, this new method is robust to missed detections, whereas the approach in [25] required all TOAs to be detected.

In [21], experimental results were presented to demonstrate the feasibility of localizing a mobile receiver using multipath. The experiment tested localization using ultrawideband signals in an indoor environment. The results included successful association of multipath components to scatterers using a tracking filter initialized to the true receiver position, as well as successful localization of the receiver. However, the experimental setup consisted of frequency-domain channel measurements that effectively sychronized the emitter and receiver. It is not obvious how to extend either the association or localization algorithms in [21] to the more realistic situation where emitter and receiver are not perfectly synchronized. Other past works, including [20] and [27], have also implicitly assumed that the time of emission is known, which is possible only if the emitter and receiver were synchronized. Our method does not require synchronization or even a cooperative emitter. Instead, we frame multipath RF emitter localization as a pseudoranging problem and estimate the time of emission along with the emitter position.

B. Plan of the paper

First in Section II, we give the assumptions and notation used throughout the paper. The analogy between multipath exploitation and GPS localization is introduced. In Section III, we describe the main technical contribution: a method for determining the correct association of measured TOAs to scattering surfaces. In Section IV, the analogy of localization based on multipath to the GPS problem is extended to study the dependence of the positioning accuracy on the relative positions and orientations of the receiver and the scattering surfaces. Section V describes simulations testing the performance of the proposed algorithm when subjected to a number of error sources including noise, clutter, and surface roughness.

II. Emitter Localization using Multipath TOA

A. Relative positions of emitter, scatterers, and receiver

Let $\mathbf{e}$ stand for the unknown position of the emitter in a three-dimensional volume $\mathcal{B}$. A single receiver is located at $\mathbf{r_0}$. Planar scattering surfaces $\mathcal{S}_i,\ i \in 1 \dots N$, are present at known positions. The position of the receiver $\mathbf{r_0}$ is assumed to be known accurately. The information about scatter positions is assumed to have been obtained previously or to be derived from other sensor measurements [3]. Additional scattering occurs from clutter objects that are not known to the localization program.

The simulations in Section V refer to the urban canyon scattering geometry shown in Figure 1(a), but the method is more generally applicable.

B. Signal and propagation model

Suppose an RF emitter broadcasts a pulse, $s(t)$ at baseband, at time b. We do not assume, as in [20], that the time of emission b can be known with arbitrary precision, even if the emitter is cooperative. We assume that only one emitter is broadcasting at a time, or that signals from multiple emitters can be disambiguated prior to performing localization.

The receiver consists of a single, omnidirectional antenna and thus provides no angle-of-arrival information. The only measurement available to the localization system is the superposition of M signals: the emitted signal that propagates along the line-of-sight path plus M multipath components.

$$w(t) = \sum_{i=1}^{M} \Gamma_i s\big(t - (t_i - b)\big) + \omega(t) \tag{1}$$

where $s(t)$ is the emitted waveform at baseband, t_i is the time-of-arrival of the ith multipath component, b is the time of emission (so $(t_i - b)$ is the propagation delay along the ith path from emitter to receiver), Γ_i is a complex factor that captures path-loss, the phase factor from the carrier, and reflection coefficients, as applicable. $\omega(t)$ is a noise process.

We assume that the emitted pulse $s(t)$ has a shape known to the receiver, either because the emitter is a bug intentionally placed on the tracked target, or the emission is produced in the operation of a standardized communication system, or we are otherwise cooperating with the emitter. As a result, a matched filter can be used to determine the TOAs of the different multipath components.

After matched-filtering, the receiver identifies a number of peaks in the response. Ideally, these peaks, $\{t_i,\ i = 1 \dots M\}$,

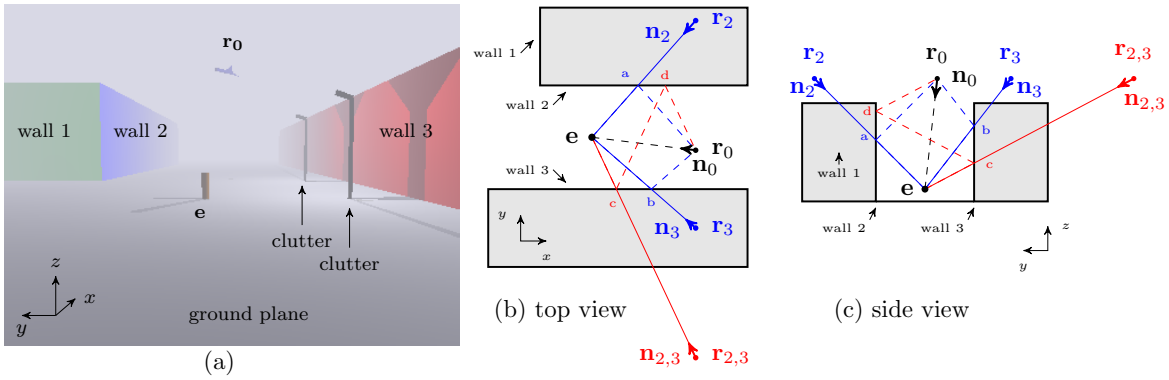

Fig. 1: In (a) is shown a rendering of the urban canyon geometry tested in the simulation experiments. The emitter position is labeled '$\mathbf{e}$', and is located just above street-level, with buildings on either side of the street. The single receiver is at '$\mathbf{r_0}$'. Multipath scattering occurs from the known ground and wall surfaces, as well as from clutter objects, whose positions may be unknown to the localization program. Diagrams (b,c) show the urban canyon geometry from the top and side, respectively. (b-c) show two single-bounce paths in blue; those signals scatter from points marked a and b. An double-bounce path with bounces at points c and d is indicated in red. The unit vectors $\{\mathbf{n_0}, \mathbf{n_2}, \mathbf{n_3}, \mathbf{n_{2,3}}\}$ play a role in the computation of GDOP, which is discussed in Section IV.

correspond to the TOAs of signals that propagated either along the line-of-sight or along one of the reflected paths. However, the localization algorithm in this paper is able to handle missing peaks, as well as components that arrive too close in time to be resolved.

C. Number of measurements and unknowns

If the objective is to locate a stationary target in three-dimensional space, then we must estimate the (x, y, z) position of the emitter, as well as the time of emission, b. To solve for these four unknowns requires at least four TOA measurements. As will be seen in Section III, determining the correct association of measured TOAs to scattering surfaces requires at least one additional constraint. Thus, at a minimum, we must detect five TOAs: the arrival along the direct path as well as arrivals from at least four non-line-of-sight (NLOS) paths. Consider the geometry shown in Figure 1(a). This geometry typically produces scattering from only three surfaces: the ground and the walls of buildings at either side of the street. Thus, considering only multipaths with a single bounce will not yield a sufficient number of measurements for performing association and localization. This motivates us to consider double-bounce paths in addition to single-bounce multipaths. M will denote the number of TOAs actually observed.

D. Describing multipath propagation using virtual receivers

The method of images has been used extensively to understand multipath in both passive and active radar systems, analyzing for example multipath from ground bounce, or multipath from ionospheric interactions in over-the-horizon radar [12]. In the case of paths that reach the receiver from the emitter after a single specular reflection (i.e. single-bounce multipath at a known, planar scattering surface), the method of images can be used to compute a virtual receiver that would measure the same TOA in the absence of scattering. With repeated application of the same concept, the virtual receivers corresponding to multipath with larger number of bounces are readily obtained.

Consider Figure 2. Let the reflecting surface $\mathcal{S}_i,\ i = 1, 2$ be described by the planar equation in the Cartesian coordinate system as $\mathbf{a_i}^T\mathbf{x} = 0$, where $\mathbf{x} := [x, y, z, 1]^T$, and $\mathbf{a_i} = [a_i, b_i, c_i, d_i]^T$. The normal to surface $\mathcal{S}_i$ is denoted $\mathbf{s_i} = \bar{\mathbf{a}}_\mathbf{i}/||\bar{\mathbf{a}}_\mathbf{i}||,\ \bar{\mathbf{a}}_\mathbf{i} = [a_i, b_i, c_i]^T$. The receiver position is denoted by $\mathbf{r_0} = [x_0, y_0, z_0]^T$. The position of a virtual receiver corresponding to a single-bounce multipath involving scattering surface $\mathcal{S}_i$ will be denoted $\mathbf{r_i},\ i = 1 \ldots N$. Using elementary algebra, it may be shown that:

$$\mathbf{r_1} = \mathbf{P_1 r_0} - 2\frac{d_1}{||\bar{\mathbf{a}}_\mathbf{1}||}\mathbf{s_1} \tag{2}$$

$$\mathbf{P_1} = \mathbf{I} - 2\mathbf{s_1 s_1}^T \tag{3}$$

where $\mathbf{P_1}$ is the Householder transformation matrix w.r.t. surface $\mathcal{S}_1$. Similarly, the coordinates of the virtual receiver corresponding to a double-bounce path, $\mathbf{r_{1,2}}$, are

$$\mathbf{r_{1,2}} = \mathbf{P_2 r_1} - 2\frac{d_2}{||\bar{\mathbf{a}}_\mathbf{2}||}\mathbf{s_2} \tag{4}$$

$$= \mathbf{P_2}\left(\mathbf{P_1 r_0} - 2\frac{d_1}{||\mathbf{a_1}||}\mathbf{s_1}\right) - 2\frac{d_2}{||\bar{\mathbf{a}}_\mathbf{2}||}\mathbf{s_2} \tag{5}$$

where $\mathbf{P_2}$ is the Householder matrix w.r.t. surface $\mathcal{S}_2$. Relevant properties of the Householder matrix are discussed in [30].

The notation $\mathbf{r_{i,j}}$ with two subscripts $i, j \in 1 \ldots N,\ i \neq j$ will be used to denote the position of second-order virtual receiver, when the order of scattering matters. In particular, $\mathbf{r_{i,j}}$ is the position of a virtual receiver corresponding to a multipath component scattering from surfaces $\mathcal{S}_j$ followed by $\mathcal{S}_i$. It is noted $\mathbf{r_{1,2}}$ is a function of $\mathbf{r_1}$, this is, because the 'latest' reflection comprising the double-bounce multipath is at surface $\mathcal{S}_1$ succeeding the reflection at $\mathcal{S}_2$. When the order of reflections are interchanged, then (4) will in general be different. In the special case of a pair of mutually-orthogonal surfaces, the second-order virtual receiver positions are identical after interchanging the order of scattering,

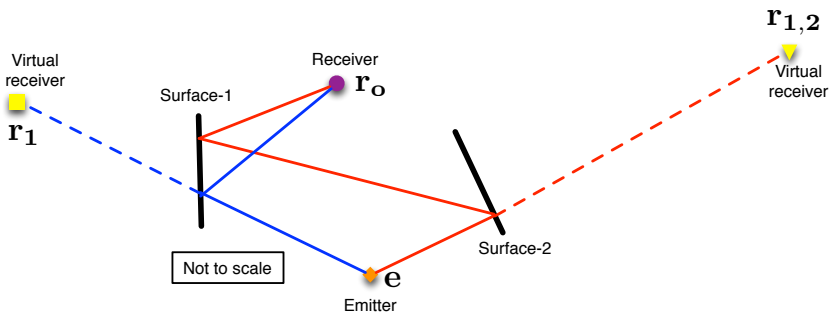

Fig. 2: The figure depicts two reflecting surfaces, the second surface is oblique w.r.t the first. One single bounce (blue) multipath and one candidate double bounce (red) multipath are shown. In the figure, the emitter (◊), physical receiver (◯), the virtual receiver from single bounce (□), the virtual receiver from double bounce multipath (▽) are seen. The dashed lines indicate the imaginary line of sight from the emitter to the virtual receivers.

As an example, in Figure 1(c) the path marked with a dashed red line leaves the emitter at $\mathbf{e}$, is reflected by the surface $\mathcal{S}_3$ at the point labeled 'c', and then from surface $\mathcal{S}_2$ at the point labeled 'd', and finally reaches the receiver located at point $\mathbf{r_0}$. This path has the same length as the straight path from $\mathbf{e}$ to $\mathbf{r_{2,3}}$, where $\mathbf{r_{2,3}}$ is computed by reflecting $\mathbf{r_0}$ about wall $\mathcal{S}_2$ and then about wall $\mathcal{S}_3$. Furthermore, the angles of this path with respect to the scattering surfaces satisfy the constraints given by Fermat's principle.

By taking the image of the true receiver $\mathbf{r_0}$ and applying the Householder technique using each scattering surface, the constellation of virtual receivers associated with single-bounce paths is obtained. By repeating this reflection procedure, starting with the virtual receivers and reflecting these each about a second surface, we can obtain the virtual receivers corresponding to double-bounce paths.

E. Bancroft algorithm applied to multipath exploitation

The basic form of the localization problem in the Global Positioning System (GPS) involves the calculation of the position and clock-offset of a mobile station based on known positions of a number of satellites. In GPS, the reference clocks onboard the satellite are highly precise. However, the clocks typically available on a mobile station are of insufficient accuracy to determine absolute ranges based on propagation time of the GPS signals, thus it is essential to estimate the offset of the mobile station clock with respect to the satellite clocks. The time-of-arrival of the signal from a particular satellite is equal to the time of emission (which is encoded in the transmission), plus the range from satellite to receiver divided by the propagation speed, plus the unknown offset of the mobile station clock. The difference between the measured time-of-arrival and the time-stamp, multiplied by the propagation speed, is called a *pseudorange* in the GPS literature. The Bancroft algorithm [2] is a classical method for processing a set of measured pseudoranges into an estimate of the mobile station position and clock offset.

In our proposed multipath exploitation localization system, it is the mobile station that emits an RF signal. As described in the previous section, propagation paths can be associated with equivalent virtual receiver positions; in our system, these virtual receivers take the place of GPS satellites. The complex waveform is received at the point $\mathbf{r}_0$. This waveform is processed using a matched filter and the peaks in the filter output are detected. Ideally, these peaks correspond to the TOAs of the various multipath components. The first TOA is that of the signal component that propagated along the direct, line-of-sight path. It is given by:

$$t_0 = b + d(\mathbf{e}, \mathbf{r_0})/c, \tag{6}$$

where $d(\mathbf{e}, \mathbf{r_0})$ is the distance from the emitter position $\mathbf{e}$ to the receiver position and b is the time shown on the receiver clock at the unknown instant of the emission. Because b is unknown, ct_0 is a pseudorange measurement. By the construction given in the previous section, the subsequent TOAs are equal to

$$t_i = b + d(\mathbf{e}, \mathbf{r_i})/c, \quad i = 1, \ldots, M, \tag{7}$$

where $\mathbf{r_i}$ is the position of the virtual receiver associated with the .

Unlike localization methods that rely on several spatially-distributed sensor nodes such as [1], [11], [13], [20], [23], [33], in this paper, we *can* assume that all the receiver clocks are perfectly synchronized. In GPS, synchronization is achieved through the use of atomic clocks onboard the satellites; in our system the virtual receivers clocks are synchronized because they are in fact co-located at the single real receiver. Thus, there is only one clock offset b to be estimated instead of a different clock offset for each receiver, . The localization problem inherent in single-sensor multipath exploitation is therefore exactly analogous to the GPS problem, so we are able to use the Bancroft estimator as the core of our localization algorithm.

F. Localization algorithm

There are four sub-parts of the multipath-exploitation localization algorithm:

1) Given the measured signal at the single real receiver (Eq. 1), estimate the TOA of each multipath component.
2) Compute the positions of the virtual receivers using the Householder transformation described in the previous section.

3) Associate the arrival times to known scatterers/virtual receivers. Some multipath components may be produced by unknown clutter in the environment; those TOAs must be identified and discarded. Once the association step is complete, there are TOAs associated with a set of spatially-distributed virtual receivers.
4) Use the Bancroft algorithm to process the TOAs at the set of spatially-distributed virtual receivers into an estimate of the target position and time of emission.

The specifics of Step 1 are beyond the scope of this paper. If the emitted signal is of sufficient bandwidth, detecting peaks in the output of a matched filter may give acceptable estimates for the TOA values [9]. In lower bandwidth settings, specialized methods developed to estimate multipath channel parameters, for example [10], [16], [18], may be appropriate. Step 2 was described in the previous section. The primary focus of the remainder of the paper is on Steps 3-4.

III. The association problem

After the set of virtual receivers have been defined using the method described in Section II-D, the important remaining difference between the single-sensor multipath exploitation problem and a localization problem based on TOAs at multiple receivers is that, a priori, it is not known which measured TOA corresponds to which virtual receiver. In more complicated scattering geometries, the subset of paths that actually permit propagation from the emitter to the receiver is also unknown. Similar problems occur when multipath information is exploited in active radar systems, as described in [25]. However, the approach used to solve the association problem in [25] is not applicable here, because that approach relied on relationships between the lengths of direct, first, and second-order multipaths, which are true for the case of a radar system, but not for a passive system for locating RF emitters.

In this paper, we consider the possibility that two or more multipath components may arrive too close in time to be resolved by the receiver matched filter. In this case, it is necessary to allow association of a single measured TOA value to more than one virtual receiver. Even more significantly, the proposed association method is robust in the face of some missed detections and can ignore TOA values produced by clutter.

A. A residual test

The solution to the association problem is based on using the Bancroft algorithm to determine position estimates for candidate associations. The candidate associations and corresponding position estimates are then ranked on the basis of a residual test, and the solution producing the smallest residual is selected. A residual test was used by [6] in a localization problem using multiple TOA values to locate a mobile station in an unknown scattering environment. Specifically, this test was used to determine which subset of TOA values measured at a constellation of receivers corresponded to propagation along a line-of-sight (LOS) path from the emitter. TOA values from non-LOS paths were then discarded to improve the accuracy of localization. Our residual test is different from the one in [6] because it operates in the TOA domain rather than in spatial coordinates, and it has a different object: to discriminate between the correct and incorrect associations rather than to determine the subset of LOS measurements.

Let the measurement equation for the times-of-arrival at the virtual receivers $\mathbf{r}_i,\ i = 1 \ldots M$, be:

$$\begin{aligned} t_i &= \tau_i + \epsilon_i \\ &= \left(b + \frac{1}{c}\sqrt{(e_x - r_{i,x})^2 + (e_y - r_{i,y})^2 + (e_z - r_{i,z})^2} \right) + \epsilon_i, \end{aligned} \tag{8}$$

Here, ϵ_i is a TOA measurement error caused by noise in the received signal. We will assume ϵ_i is Gaussian with mean zero and variance σ_i^2. The variance is determined by the performance of the matched filter estimator for TOA values and depends on the underlying signal characteristics.

Let $\mathcal{G}$ be a particular candidate association of TOA values to virtual receivers. Using this association, we can apply the Bancroft algorithm to obtain a candidate estimate for the position and time of emission: $(\mathbf{e}^{\mathcal{G}}, b^{\mathcal{G}}) := (e_x^{\mathcal{G}}, e_y^{\mathcal{G}}, e_z^{\mathcal{G}}, b^{\mathcal{G}})$. Now, define the residual $\epsilon_i^{\mathcal{G}}$ to be the difference between the ith measured TOA, t_i, and the TOA value $\tau_i^{\mathcal{G}}$ predicted by the scattering model using the candidate emitter position and clock offset:

$$\begin{aligned} \epsilon_i^{\mathcal{G}} &= t_i - \tau_i^{\mathcal{G}} \\ &= t_i - \left(b^{\mathcal{G}} + \frac{1}{c}\sqrt{(e_x^{\mathcal{G}} - r_{i,x})^2 + (e_y^{\mathcal{G}} - r_{i,y})^2 + (e_z^{\mathcal{G}} - r_{i,z})^2} \right). \end{aligned} \tag{9}$$

The Bancroft method finds the emitter position and clock offset that minimizes $\sum_i (\epsilon_i^2/\sigma_i^2)$ [2]. In the case that $\mathcal{G}$ is the correct association, then the only errors are due to the TOA measurement noises ϵ_i. In that case, the sum of the normalized squared residuals

$$\chi^2_{\mathcal{G}} = \sum_i \frac{(\epsilon_i^{\mathcal{G}})^2}{\sigma_i^2} \tag{10}$$

follows a chi-squared distribution with $K - 4$ degrees of freedom, where $K \leq M$ is the number of TOA measurements actually incorporated in the position estimate, and 4 is the number of free parameters of the localization solution in 3D space. If $\mathcal{G}$ is not the correct association of TOA values to virtual receivers, there will be additional errors in the residual, and $\chi^2_{\mathcal{G}}$ will deviate from the expected chi-square distribution. Under suitable conditions, this deviation can be used to identify the correct association among a large number of candidate associations.

B. Solution to the association problem

In this section, we present the details of a two-stage algorithm to solve the association problem. The first stage reduces the number of candidate associations by discretizing the physical search space and finding a subset of emitter positions and times of emission that yield plausible associations with the measured data. In the second stage, the position estimates from the first stage (whose precision is limited by the fineness of the discretization) are refined to obtain the residual error statistic described in the previous section. This residual is used to determine which of the plausible associations selected by the first stage is most likely correct.

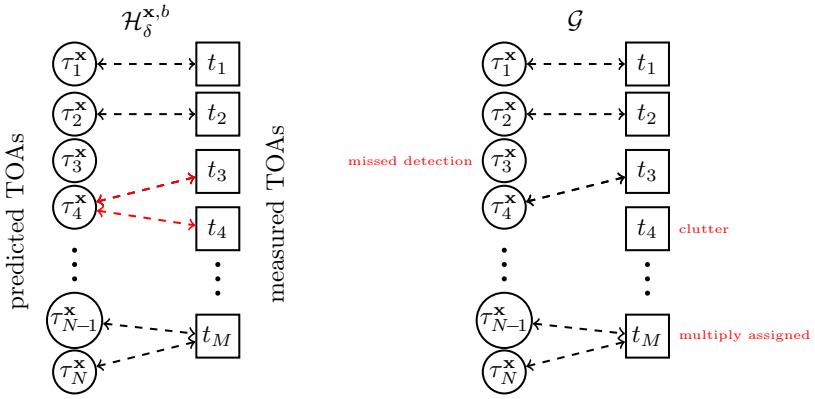

Fig. 3: At left is a bipartite graph $\mathcal{H}_\delta^{\mathbf{x},b}$ representing plausible associations of TOAs to paths. The values $\{\tau_1^{\mathbf{x},b},\ldots,\tau_N^{\mathbf{x},b}\}$ are predicted TOAs, sorted in increasing order. The values $\{t_1,\ldots,t_M\}$ are measured TOAs, also in increasing order. Edges of $\mathcal{H}_\delta^{\mathbf{x},b}$ are tentative associations made by testing if $|t_i-\tau_j^{\mathbf{x},b}|<\delta$. In this scenario, there is no measured TOA that associates with the predicted TOA $\tau_3^{\mathbf{x},b}$. Two TOAs are tentatively associated with $\tau_4^{\mathbf{x},b}$; at least one of these must be erroneous, so both possibilities must be tested. The last measured TOA has been associated with both the last two virtual receivers; this is a case of multiple assignment, which is permitted to account for situations where two multipath components are not resolvable in time. At right is one subgraph $\mathcal{G}\subseteq\mathcal{H}_\delta^{\mathbf{x},b}$ satisfying the conditions given in the text.

A direct, brute-force search through all associations of K out of the M measured TOAs would require testing $\binom{N}{K}\times\binom{M}{K}$ candidate associations, where N is the number of known virtual receivers positions and M is the number of measured TOAs. The brute-force approach is prohibitive for all but the simplest, clutter-free cases. The solution we propose greatly reduces the number of candidate associations that must be checked at the price of a small probability that the correct association will be discarded by the first stage of the algorithm. As we will show, this probability of missing the correct association can be computed and controlled through an appropriate choice of the plausibility threshold used to pre-screen candidate associations. This approach is also helpful for distinguishing clutter returns and discarding them without a combinatorial increase in computational cost.

The first step is to discretize the search space in which the emitter is to be found. We assume that the search volume $\mathcal{B}$ can be bounded using The edge length of the discretization cells, D, should be selected to obtain a reasonable computation time.

Let $\mathbf{x}$ be the center of a discretization cell. For a fixed $\mathbf{x}$, only certain virtual receivers will be active in the sense that they correspond to valid propagation paths from $\mathbf{x}$ to the true receiver position $\mathbf{r}_0$.

The next step is to determine candidate values for the time of emission using a gridding and cross-correlation procedure. This step may be unnecessary if the direct path TOA, t_0, is present and can be distinguished from the other TOAs based on signal power. If this is the case, this knowledge can be used to make a preliminary estimate of the time of emission: $\hat{b}=t_0-d(\mathbf{x},\mathbf{r_0})/c$. If this is not the case, a gridding procedure can be used to identify candidate times of emission that yield predicted TOAs with sufficient overlap with the set of measured TOAs. Compute predicted TOA values using an arbitrary b:

$$\tau_i^{\mathbf{x},b}=b+d(\mathbf{x},\mathbf{r}_i)/c,\quad i=0\ldots N, \tag{11}$$

Then construct a vector $\mathbf{p}$ whose jth entry counts the number of predicted TOAs in the range $[(j{-}1)T,(j{+}1)T]$, where T is the temporal discretization step. Similarly, construct a vector $\mathbf{m}$ corresponding to the measured TOAs. For the measured TOA discretization vector, the jth entry should be one or zero, depending on if there is at least one measured TOA in the range $[(j{-}1)T,(j{+}1)T]$. Finally, compute the cross-correlation of $\mathbf{p}$ and $\mathbf{m}$, and identify those offsets $\hat{b}$ where the cross-correlation function is greater than or equal to K. For each offset, recompute $\tau_i^{\mathbf{x},b}$ using Eq. 11. This procedure allows the assignment of one measured TOA to multiple virtual receivers, but does not double-count virtual receivers that could plausibly associate with multiple measured TOAs.

Next, we construct a bipartite graph $\mathcal{H}_\delta^{\mathbf{x},b}$ that indicates the set of plausible associations for an emitter at $\mathbf{x}$, and time of emission b. The first set of graph nodes are measured TOA values; the second node set includes predicted TOA values. $\mathcal{H}_\delta^{\mathbf{x},b}$ has an edge between a node t_i in the first node set and $\tau_j^{\mathbf{x},b}$ in the second node set if $|t_i-\tau_j^{\mathbf{x},b}|$ is less than a predetermined threshold δ. An example plausible association graph is shown at left in Figure 3.

The association threshold δ determines the number of plausible association graphs that will have to be tested and hence is a major factor in determining the processing time of the localization algorithm. A reasonable value of δ should take into account the size of the discretization cell, as well as the size of the systematic errors and noise affecting the TOA measurements. The probability that the correct association will be missed because the errors exceed the threshold δ for all discretization cells is shown in Figure 4. The probabilities were computed using Monte Carlo integration under the assumption that the distance from the emitter to the virtual receivers is much greater than D. This figure can be used to select the

smallest value of δ that will deliver an acceptable probability of missing the correct association.

Finally, we want to find a subgraph $\mathcal{G} \subseteq \mathcal{H}_\delta^{\mathbf{x}}$ such that:

1) nodes in the set of predicted TOAs have degree 0 or 1,
2) the number of edges in $\mathcal{G}$ is K or greater.

Nodes in the set of measured TOAs may have arbitrary degree. It is then necessary to solve the localization using the Bancroft algorithm for each association subgraph $\mathcal{G} \subseteq \mathcal{H}_\delta^{\mathbf{x}}$ satisfying the conditions (1-2), and for each cell of the discretization grid. For each solution, the sum of squared residuals $\chi^2_{\mathcal{G}}$ should be computed and stored. At the end, the estimated position that gave the smallest $\chi^2_{\mathcal{G}}$ is selected. The search through subgraphs $\mathcal{G}$ with more than K edges was conducted by greedily discarding the predicted TOA node that contributed most to the residual of the best association found so far.

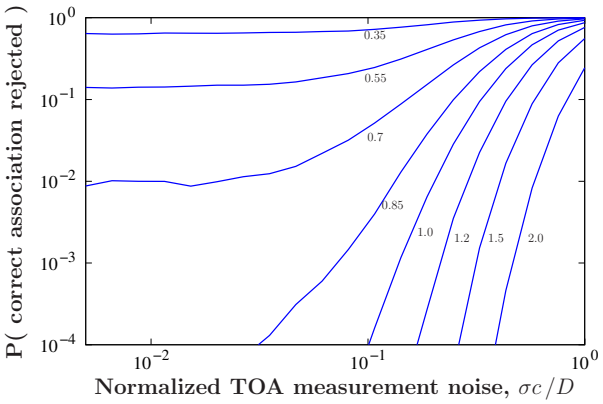

Fig. 4: The plot shows the probability that the correct association of measured TOAs to virtual receivers will not be deemed plausible, and thus will never be checked. The curves give this probability for plausibility thresholds $\delta = \{0.35D, \ldots, 2D\}$. Both σ and δ are normalized with respect to D, the edge-length of the discretization cell. Picking the smallest δ that achieves the desired performance reduces computation time.

IV. Precision of Localization

In this section, we state the Cramér-Rao lower bound (CRLB) on the positioning accuracy that can be obtained using the multipath exploitation algorithm in the presence of TOA measurement errors. Because of the analogy between multipath exploitation and the localization problem faced in satellite navigation systems, the same CRLB given in [2] applies here.

Geometric dilution of precision (GDOP) is a concept used in the GPS community to characterize the loss in positioning accuracy caused by unfavorable configurations of the satellites with respect to the mobile station. We given an example of how the GDOP varies with the receiver position in the urban canyon geometry, and suggest how this could be used to maximize localization performance.

A. Cramér-Rao lower bound on precision of localization

Suppose the times-of-arrival t_i at a number of (real or virtual) receivers $\mathbf{r_i}$ are measured according to Eq. 7, but with an error ϵ produced by the effect of noise in the cross-correlation receiver. This error is assumed to be Gaussian .

$$t_i = b + d(\mathbf{e}, \mathbf{r_i}) + \epsilon_i, \quad \forall i = 1 \ldots M, \tag{12}$$

$$\mathcal{E}(\epsilon_i) = 0, \quad \mathcal{E}(\epsilon_i \epsilon_j) = \delta_{ij}\sigma_i^2, \tag{13}$$

where $\mathcal{E}(X)$ denotes the expectation of random variable X. Let $\hat{\mathbf{y}} = (\hat{\mathbf{e}}^T, -\hat{b})^T$ be the concatenation of the estimated emitter position and the estimated time of emission. If the Bancroft algorithm is applied to multipath TOA measurements $\{t_1, \ldots, t_M\}$ affected by independent Gaussian errors as in Eq. 13, then the variance of the estimated position and time of emission, $\mathbf{\Sigma}$, are bounded below by the CRLB [2]:

$$\mathbf{\Sigma} = \mathrm{var}(\hat{\mathbf{y}}) \succeq \left(\mathbf{H}^T \mathbf{W} \mathbf{H}\right)^{-1}, \tag{14}$$

where $\mathbf{H}$ is the matrix

$$\mathbf{H} = \begin{pmatrix} \mathbf{n}_1^T & -1 \\ \vdots & \vdots \\ \mathbf{n}_N^T & -1 \end{pmatrix} \tag{15}$$

obtained by computing a first-order variation in the pseudo-ranges measurements with respect to changes in the emitter position. That is, $\mathbf{n}_i = \partial t_i / \partial \mathbf{e}$, which gives a vector pointing from the emitter $\mathbf{e}$ to the virtual receiver position $\mathbf{r}_i$. Finally, $\mathbf{W} = \mathrm{diag}\left(\frac{1}{\sigma_0^2} \cdots \frac{1}{\sigma_M^2}\right)$ is the diagonal matrix of the inverses of the TOA measurement variances.

A different CRLB for wideband TDOA-based localization was derived in [28] and applied to multipath localization in [27]; the difference comes about because in those papers, the time of emission of the RF signal was implicitly assumed to be known.

B. Example: optimal receiver position in an urban canyon

The geometric dilution of precision (GDOP) is defined to be the trace of the matrix $(\mathbf{H}^T\mathbf{H})^{-1}$ [2]. Whereas the CRLB depends on the characteristics of the RF signal through the TOA measurement uncertainty matrix $\mathbf{W}$, GDOP is a signal-independent measure of the magnification of errors that occur when TOA measurements are processed into a position estimate. Because in an adverserial situation the signal characteristics are out of the control of the receiver, in this section, we consider how the receiver should position itself to minimize GDOP. By doing so, it achieves good localization performance regardless of the emitted signal.

Let the emitter be located at ground level at $\mathbf{e} = (0, 0, 0)$. Two walls at $y = \pm 10$ meters together with the ground plane at $z = 0$ form an urban canyon extending in the x-direction. Figure 5 shows the GDOP for localization based on the direct path and two single-bounce paths, using the constraint that the emitter is at ground level. The GDOP is shown for a fixed receiver elevation of $z = 5$ m and a range of (x, y) coordinates. The position of the receiver that minimizes GDOP is near $\mathbf{r}_0 = (6.5, 0, 5)$. Not shown is an identical minimum when $\mathbf{r}_0 = (-6.5, 0, 5)$. The GDOP becomes very large as the receiver position approaches the plane $x = 0$, where the emitter and all virtual receivers are coplanar. This result has interesting implications for an optimal search strategy in the

TABLE I: Association algorithm

- Select parameters $D > 0, T > 0$, $\delta > 0$ and $K \geq 5$, which control the spatial discretization, the temporal discretization, the initial error in TOA measurement considered plausible and the minimum number of TOAs to use in positioning.
- Compute the constellation of virtual receiver positions $\{\mathbf{r_i}, \mathbf{r_{i,j}}\}$, $\forall i, j \in 1 \ldots N$, using the Householder transformations.
- Construct a vector $\mathbf{m}$ whose jth entry is one if there is at least one measured TOA in the range $[(j-1)T, (j+1)T]$, and zero otherwise.
- Discretize the search space $\mathcal{B}$ into cells of side-length D.
- For each discretization point $\mathbf{x} \in \mathcal{B}$:
  1) Compute the subset of virtual receivers visible from $\mathbf{x}$.
  2) For each visible virtual receiver, compute predicted values for TOAs using Eq. 11, with the discretization point $\mathbf{x}$ and arbitrary value for the time of emission, $\hat{b}_0^{\mathbf{x}}$. Construct a vector $\mathbf{p}$ whose jth entry counts the number of predicted TOAs in the range $[(j-1)T, (j+1)T]$.
  3) Compute the cross-correlation between the measurement time vector $\mathbf{m}$ and the discretized predicted time vector $\mathbf{p}$.
  4) For every time-offset b that produces at least K correspondences between $\mathbf{m}$ and $\mathbf{p}$,
     a) Recompute $\tau_i^{\mathbf{x},b}$ using Eq. 11 with the estimated time-offset b.
     b) Form an initial association graph $\mathcal{H}_\delta^{\mathbf{x},b}$ by connecting nodes $\tau_i^{\mathbf{x},b}$ and t_j if $|t_i - \tau_j^{\mathbf{x},b}| < \delta$.
     c) Any measured TOAs t_j whose node in $\mathcal{H}_\delta^{\mathbf{x}}$ has degree 0 can be provisionally labelled as clutter. Any predicted TOAs $\tau_i^{\mathbf{x}}$ whose node has degree 0 can be provisionally labelled as missed detections.
     d) Let $V_{>0}^{\mathbf{x}}$ be the subset of predicted TOA nodes in $\mathcal{H}_\delta^{\mathbf{x}}$ with degree > 0. While there are at least K nodes in $V_{>0}^{\mathbf{x}}$,
        i) If any nodes of $V_K^{\mathbf{x}}$ has degree greater than 1, iterate over all selections of a single edge for those nodes. This gives an association graph $\mathcal{G} \subseteq \mathcal{H}_\delta^{\mathbf{x}}$ satisfying the conditions given in the text.
           A) Use Bancroft method to compute a predicted position $\mathbf{e}^{\mathcal{G}}$ and clock offset $b^{\mathcal{G}}$ using the association given by $\mathcal{G}$.
           B) Recompute predicted TOAs using Eq. 11.
           C) Compute the residual $\chi^2_{\mathcal{G}}$ using Eq. 10.
           D) Store the association graph $\mathcal{G}$, the estimates $\mathbf{e}^{\mathcal{G}}$ and $b^{\mathcal{G}}$, and the residual $\chi^2_{\mathcal{G}}$.
        ii) Pick the association $\mathcal{G}$ that produced the smallest total residual. If number of edges $\mathcal{G}$ exceeds K, discard the node in $V_{>0}^{\mathbf{x}}$ that contributes most to the residual $\chi^2_{\mathcal{G}}$.
- Pick the association and estimated target position that produced the smallest residual.

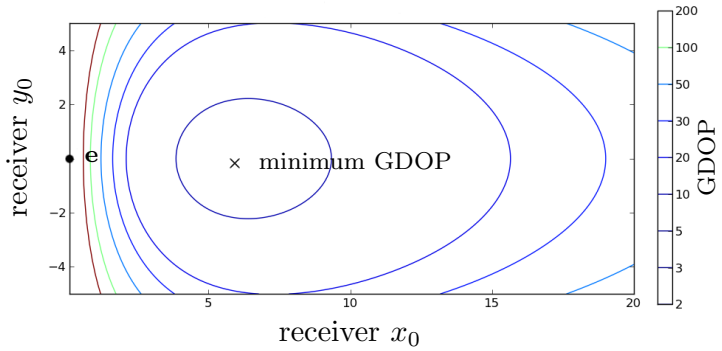

Fig. 5: The contour plot shows the GDOP computed for various positions of the real receiver $\mathbf{r}_0 = (x_0, y_0, z = 5)$. The emitter is located at $\mathbf{e} = (0, 0, 0)$. The geometry is similar to the urban canyon in Figure 1: two walls are located at $y = \pm 10$ and have their extent along the x direction. The minimum GDOP occurs near $\mathbf{r}_0 = (6.5, 0, 5)$.

case that some prior information about the emitter position is available. The receiver should not directly approach the predicted emitter position, as that will produce a constellation of virtual receivers giving the worst localization performance.

V. Simulations

This section describes three simulations that incorporate varying levels of realism. The first shows the performance of the localization algorithm in an idealized scenario with TOA measurement errors, but without clutter or wall roughness. The second experiment incorporates a model for wall roughness and shows the effect that this has on determining the correct association solution as well as the positioning accuracy. The final experiment includes returns from clutter and shows the ability of the algorithm to reject TOA measurements corresponding to unmodeled scatterers, while retaining those that do allow localization of the emitter using known scattering surfaces.

A. Effect of TOA Measurement Errors

This simulation tests the ability of the proposed method for distinguishing the correct association of measured TOAs to virtual receivers from incorrect associations. It also compares the RMS positioning error (RMSE) to the lower bound given by the CRLB. This simulation was conducted using several emitter and receiver positions in the urban canyon geometry, as shown in Figure 6(a,b).

Single- and double-bounce paths were considered. Depending on the particular emitter and receiver position, between five and seven propagation paths were available. Times-of-

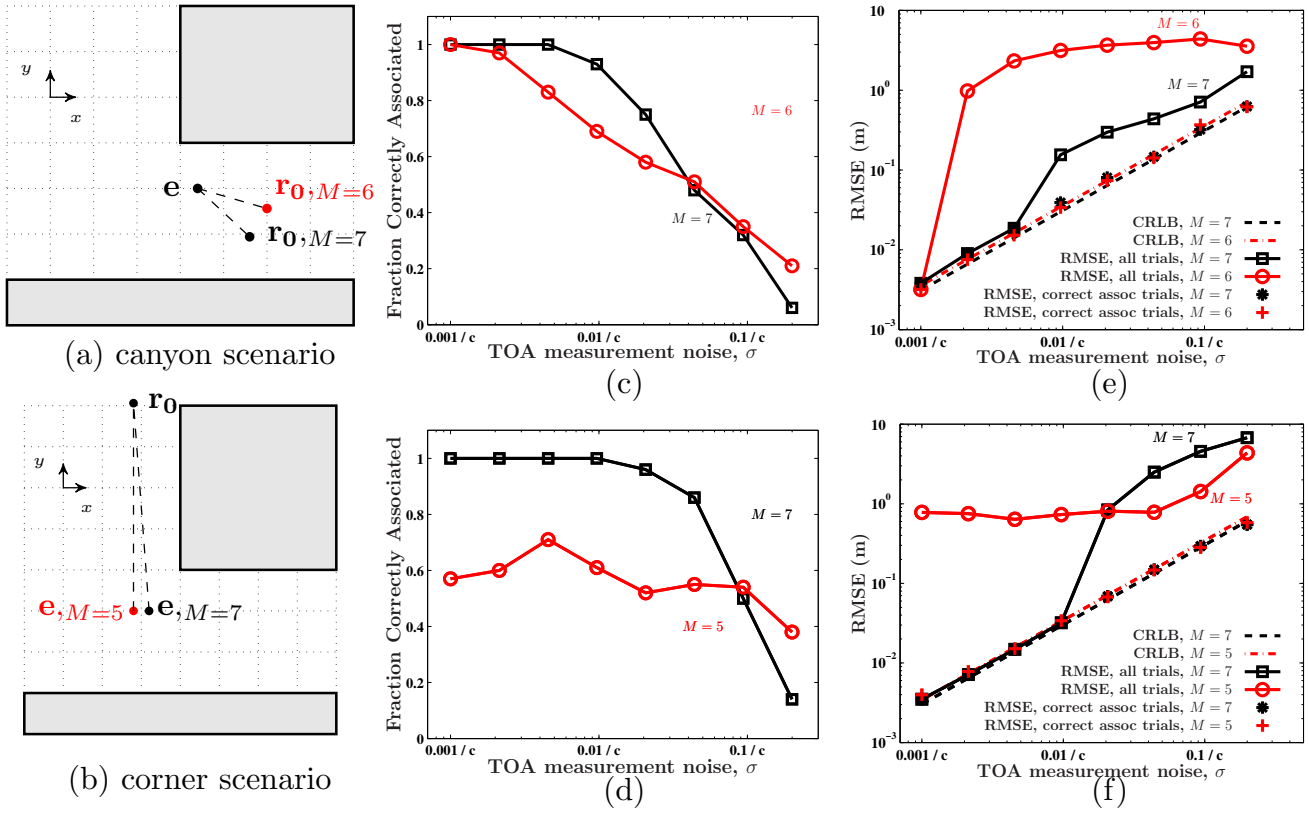

Fig. 6: At left, (a,b) show the positions of the emitter $\mathbf{e}$ and receiver $\mathbf{r_0}$ in four scenarios with varying number ($M = 5, 6, 7$) of active propagation paths. The scene has dimensions of 40×40 meters; the grid indicates divisions of 5 meters. In (c,d) are shown the fraction of 100 trials in which the correct association was selected, for a range of values of the TOA measurement noise. In (e,f) are plotted the RMS position error for all trials, as well as for the subset of trials where the correct association was determined. The lower bounds on RMSE predicted by the CRLB are plotted with dashed lines.

arrival were computed using the ; then measurement noise was added to the ideal TOA values. The measurement noise was zero-mean Gaussian with a standard deviations spanning the range $\sigma \in [3.3 \times 10^{-12},\ 6.7 \times 10^{-10}]$ seconds. Although this simulation directly synthesized measured TOAs, in a real system, the uncertainty of measured TOAs σ would be determined by the characteristics of the transmitted RF signal. If the TOA estimator operates near the Cramér-Rao lower bound, then σ is related to the effective signal bandwidth β and signal-to-noise ratio χ according to [9]:

$$\sigma^2 \geq \frac{1}{8\pi^2\beta^2\chi}. \tag{16}$$

For example, the σ values tested in this simulation would correspond to RF signal bandwidths in the range 30 MHz $< \beta <$ 6 GHz if the SNR is 15 dB, or the range 17 MHz $< \beta <$ 3.4 GHz if the SNR is 20 dB. This overlaps and extends to smaller bandwidths the range tested in the indoor experiments of [21].

In the canyon scenarios shown in Figure 6(a), the constellation of active virtual receivers, that is the set of virtual receivers corresponding to propagation paths actually observed, is restricted to a plane with x-coordinate equal to that of the real receiver. Because of this degenerate receiver configuration, the Bancroft method reported estimated positions to the right and to the left of the real receiver with equal probability. For the purpose of computing RMSE, estimated positions to the right of the real receiver were reflected back to the left side. In practice, it would be necessary to maintain two track hypotheses for the emitter position.

The search volumes was The discretization of the search space used cubes $D = 0.2$ m on a side. Using the results of Figure 4, the plausibility threshold δ was set for each value of σ to limit the probability of rejecting the correct assocition to $P < 0.1$. In all trials, $K = M$, so only association graphs that assigned all measured TOAs were considered.

The plots in Figure 6(c,d) shows the fraction of trials for which the minimum residual gave the correct association. In the canyon scenario, for the case where $M = 6$, the constellation of virtual receivers is nearly symmetric and thus there are occasionally incorrect associations that result in small residuals. From Figure 6(e,f), it can be seen that when the correct association was selected, the RMSE was close to the CRLB.

The empirical distribution of measured residuals, $\chi^2_{\mathcal{G}}$ under correct and the nearest incorrect associations are shown in Figure 7. The distribution of residuals under correct association are in good agreement with a chi-square distribution with three degrees of freedom, as expected for a situation with seven measurements and four solution variables. The

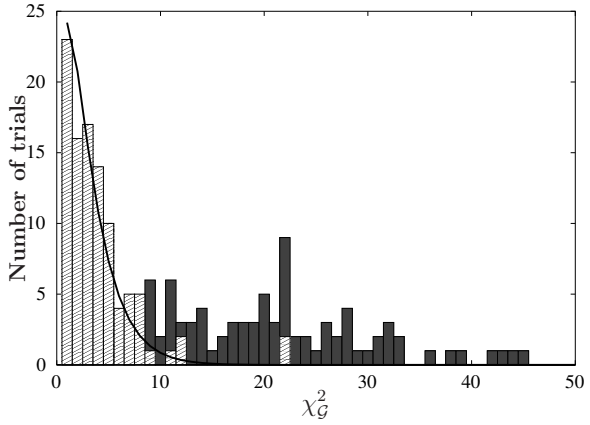

Fig. 7: The plot shows the $\chi^2_{\mathcal{G}}$ values obtained in 100 trials of the canyon scenario with 7 TOA values, with $\sigma = 0.01/c \approx 33.3$ ps. The light gray striped bars give the histogram of the minimum value of $\chi^2_{\mathcal{G}}$ found over all associations. The pdf of a chi-squared distribution with three degrees of freedom is overlaid in black, and the two are seen to be in excellent agreement. In dark gray bars is shown the histogram of the second smallest values of $\chi^2_{\mathcal{G}}$, which come from erroneous associations. The correct association was found in all trials.

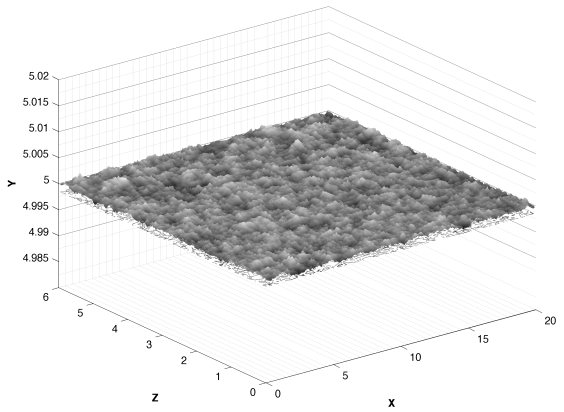

Fig. 8: Wall roughness of 1% of the operating wavelength for a carrier frequency of 10 GHz. The wall lies in the (x,z) plane with a baseline depth of $y = 5$. This plot uses $P = Q = 200$ and spatial correlation $\eta = 0.3$

result of the simulation shows that there is a wide range of threshold values that can be used to distinguish the true association, while accepting only a small number of incorrect associations. If multiple associations are accepted, it may be necessary to maintain multiple track hypotheses for the emitter. Except in degenerate geometries, the incorrect hypotheses will eventually be rejected.

B. Sensitivity of localization to wall roughness

Thus far, we have not considered the effect of wall roughness on localization. For large wavelengths, on the order of a few cm, the effect of wall roughness on the multipath is expected to be insignificant. However for shorter wavelengths in the mm range, reflections from rough walls consist of both specular and diffuse components and therefore the impact of wall roughness must be investigated. To completely address the impact of wall roughness, a full investigation using electromagnetic theory would be needed, see for example [31], [32] and references therein. Here, we take a high-level but numerically tractable signal processing approach along the lines of [22], [19]. Our wall roughness model is based on using random perturbations to model roughness, as pioneered by Rice [22], and used in [32], [31] and references therein. We first consider the effect of roughness on a multipath component involving a bouce from a single wall, and then generalize to paths involving interactions with multiple rough walls.

Consider a $P \times Q$ grid of sub-reflectors on each wall. Each sub-reflector is placed at a random depth from the baseline smooth wall. These depths are sampled from a Gaussian distribution with zero mean and a standard deviation expressed as a percentage of the system operating wavelength [19]. To simulate texture, the depths of sub-reflectors may be spatially-correlated [19], [22].

The multipath returns from the $P \times Q$ grid of sub-reflectors are superposed, with each sub-reflector contributing diffuse multipath. Rather than developing a detailed model for the electromagnetic properties of the sub-reflectors, we propose a simple but flexible model for weighting the magnitude of the signals contributed by each sub-reflector. The signal scattered by the sub-reflector indexed by (p, q), which is located at the point $\mathbf{x}_{pq}$, is weighted by

$$\mathcal{W}(p, q) = \exp(-\gamma||\mathbf{x}_{pq} - \mathbf{x}_s||), \tag{17}$$

where $\mathbf{x}_s$ is the specular reflection point on the baseline smooth wall. This weighting function is circularly-symmetric and centered at $\mathbf{x}_s$. No specular multipath is explicitly incorporated into our model; however, for large values of the weighting parameter γ, only sub-reflectors near the specular point contribute significantly to the scattered signal, and the resulting signal approaches the signal that would be scattered by a smooth wall. The phase of the contribution from each sub-reflector is proportional to the propagation time.

To model texture, the depths of the sub-reflectors (p_1, q_1) and (p_2, q_2), have a correlation coefficient given by:

$$\mathcal{R}(p_1, p_2, q_1, q_2) = \tag{18}$$
$$\begin{cases} \exp(-\eta|p_1 - p_2|)\exp(-\eta|q_1 - q_2|) & p_1 = p_2 \text{ or } q_1 = q_2 \\ 0 & \text{otherwise.} \end{cases}$$

Equation (18) implies that for a given sub-reflector, the depths of sub-reflectors on its left, right, top, and bottom are correlated, whereas other sub-reflectors are uncorrelated, even if they are in close proximity to the considered sub-reflector. Other correlation models could be used, but the model in (18) is sufficient for the investigation performed here. A wall realized according to the model is shown in Figure 8.

Modeling double-bounce diffuse multipath is similar in spirit to modeling the single-bounce diffuse multipath. Consider two rough walls, $\mathcal{S}_1$ and $\mathcal{S}_2$, comprising $P \times Q$ sub-reflectors each. The signal from the emitter is first reflected from a sub-reflector on $\mathcal{S}_1$ indexed by (p_i, q_j) and is then reflected from the sub-reflector on $\mathcal{S}_2$ indexed by (p_k, q_l). The amplitude weighting of the resulting diffuse multipath is taken

to be $\mathcal{W}(p_i, q_j)\mathcal{W}(p_k, q_l)$, where the individual $\mathcal{W}(\cdot,\cdot)$ are as in (17) with the specular points computed on their respective walls. If $s(t-b)\exp(j2\pi f_c(t-b))$ is the emitted signal, then the composite double-bounce diffuse multipath scattered from rough surfaces $\mathcal{S}_1$ and $\mathcal{S}_2$ is given by

$$\sum_{i=1}^{M}\sum_{j=1}^{N}\sum_{k=1}^{M}\sum_{l=1}^{N}\mathcal{W}(p_i,q_j)\mathcal{W}(p_k,q_l)s(t-(\tau_{ij}^{(1)}+\tau_{ij}^{(kl)}+\tau_{kl}^{(2)})-b) \cdot \exp(-2f_c(\tau_{ij}^{(1)}+\tau_{ij}^{(kl)}+\tau_{kl}^{(2)})-b)/c). \quad (19)$$

Further details are given in Table II.

Finally, the double-bounce composite multipath components scattered from all pairs of walls should be added to the composite single-bounce multipath components as well as the direct path signal. This combined signal is then match-filtered and peaks are selected from the resulting profile to obtain the rough-wall-affected TOA estimates.

Figure 9 shows the bias and standard deviation of the estimates of the emitter location and the time of emission, assuming correct association, for a range of wall-roughnesses. The parameters $\eta = 0.3$ and $\gamma = 0.6$ were used. The estimates suffer from a bias, albeit a small one. The estimator biases are on the order of 10 cm, compared with a typical search-volume dimension of tens of meters. The standard deviations for all cases are quite small, implying that the biases are persistent. Neither the bias nor the standard deviation of the estimates show a significant dependence on the wall-roughness standard deviation. In Table III(a,b), the bias and standard deviation of the emitter location estimates and the bias and standard deviation of the time of emission are shown for varying weighting parameter γ and varying correlation parameter η, respectively. It is seen that the estimator bias is sensitive to the weighting parameter γ; specifically, the bias decreases with increasing γ as a greater proportion of the diffuse scattering occurs nearer the specular point. At smaller values of γ, the diffuse scattering results in increased sidelobe levels in the output of the matched filter and more significant perturbations of the estimated times-of-arrival. Finally, the bias in the emitter position estimate is found to be insensitive to changes in the spatial correlation parameter η.

C. Clutter rejection

In this simulation we tested the ability of the association algorithm to reject TOA measurements that are produced by scattering from unknown clutter in the scene. Because the positions of the clutter objects are unknown, the corresponding TOA values cannot be used in the localization algorithm, but must be identified and discarded. We tested this problem in the three-dimensional urban canyon geometry depicted in Figure 10(a). In all trials, the receiver was located at $(12, -4, 5)$. The emitter position was varied over the entire area shown, and 10 trials were performed at each emitter position. Depending on the emitter position, there were between 4 and 12 propagation paths, counting a direct path and paths with up to two reflections on modeled scattering surfaces. The number of propagation paths for each point is shown in Figure 10(a). In addition, three point scatterers whose positions were unknown to the localization algorithm were added. These clutter scatterers produced three additional TOAs that had to be distinguished from TOAs corresponding to modeled scatterers. Multi-bounce interaction between the clutter scatterers and surfaces was not considered. Ideal TOAs were computed using , and then measurement noise was added to the ideal TOAs. The association algorithm described in Table I was applied. The algorithm did not know which TOA values were clutter, nor which TOA values were produced by which scattering surface.

For the results shown in Figure 10(b-c), the TOA measurement noise was set to 33.3 picoseconds, corresponding to a single-measurement pseudoranging uncertainty of 0.01 m. The search space was restricted to a 10×10 meter box about the true emitter position. The fineness of the discretization of the search space was 0.2 meters. The plausibility threshold was set as in the first experiment. The parameter specifying the minimum number of TOAs to be associated was $K = 6$. The effect of varying K is described later.

A solution was deemed to be the correct association if all clutter TOAs were rejected and all TOAs used in the solution were associated to the correct virtual receiver. The fraction of trials in which the correct association was determined is shown in Figure 10(b). For some emitter positions, two propagation paths were of very nearly equal length, so it was difficult to correctly assign the two corresponding TOAs that were nearly indistinguishable. For example, this occurs when the emitter position is at $y = -4$ or $y = -1$. In both these cases, the two paths involving bounces off of both walls of the canyon are equal in length. As a result, the fraction of trials in which the correct association is found falls below half. Nevertheless, the effect of switching the association of these two TOAs is minimal, and the RMSE positioning error for these emitter locations is no worse than nearby positions that do not suffer from this ambiguity.

The square in Figure 10(b) indicates an emitter position $(-5, 10, 0.6)$ for which the direct propagation path between emitter and receiver is blocked. However, 7 multipath propagation paths are available, and the algorithm correctly rejects clutter and localizes the emitter even in this non-line of sight case.

As shown in Figure 11, at measurement noise levels $\sigma = 0.005/c \approx 16.7$ ps and above, the algorithm occasionally selected an incorrect association, which resulted in estimated positions clustered about an incorrect position. These trials account for the additional positioning errors above and beyond the values predicted by the CRLB that are seen at larger σ values; when those trials are excluded the RMSE is closer to the value predicted by the CRLB. The set of virtual receivers in the urban canyon geometry result in a large GDOP, dominated by the contribution of the x-direction error. The point cloud is spread primarily along that direction.

Finally, we investigated how the robustness of the association algorithm depends on the choice of the parameter K, which sets the minimum number of associated TOAs for a solution to be considered valid. The emitter was fixed at point $\mathbf{e} = (1, -5, 0.6)$, which is marked by a circle in Fig. 10(a). The receiver was at $\mathbf{r}_0 = (12, -4, 5)$. 100 trials were

TABLE II: Algorithm for computing diffuse double-bounce multipath

1. Compute the coordinates of the specular reflection points on $\mathcal{S}_1$ and $\mathcal{S}_2$. There exists a unique double-bounce multipath eigenray from emitter to receiver consisting of specular reflections at $\mathcal{S}_1$ and $\mathcal{S}_2$ [24], [26]. Hence the specular reflection coordinates are functions of the emitter, the receiver and the locations of the baseline smooth $\mathcal{S}_1$ and baseline smooth $\mathcal{S}_2$.
2. Consider sub-reflectors (p_i, q_j) and (p_k, q_l) on surfaces $\mathcal{S}_1$ and $\mathcal{S}_2$, respectively.
3. Compute the three time delays, from emitter to sub-reflector (p_i, q_j), from (p_i, q_j) to (p_k, q_l), and from sub-reflector (p_k, q_l) to the receiver. These are denoted by $\tau_{ij}^{(1)}, \tau_{ij}^{(kl)}, \tau_{kl}^{(2)}$, respectively.
4. Obtain the diffuse multipath component, whose magnitude is $\mathcal{W}(p_i, q_j)\mathcal{W}(p_k, q_l)$, and whose phase is proportional to the sum of the computed time delays in step-3.
5. Repeat steps 1–4 with a different set of sub-reflectors until all sub-reflectors on $\mathcal{S}_1$ and $\mathcal{S}_2$ have been exhausted.
6. Coherently add all the diffuse multipath components to obtain a composite double-bounce multipath.

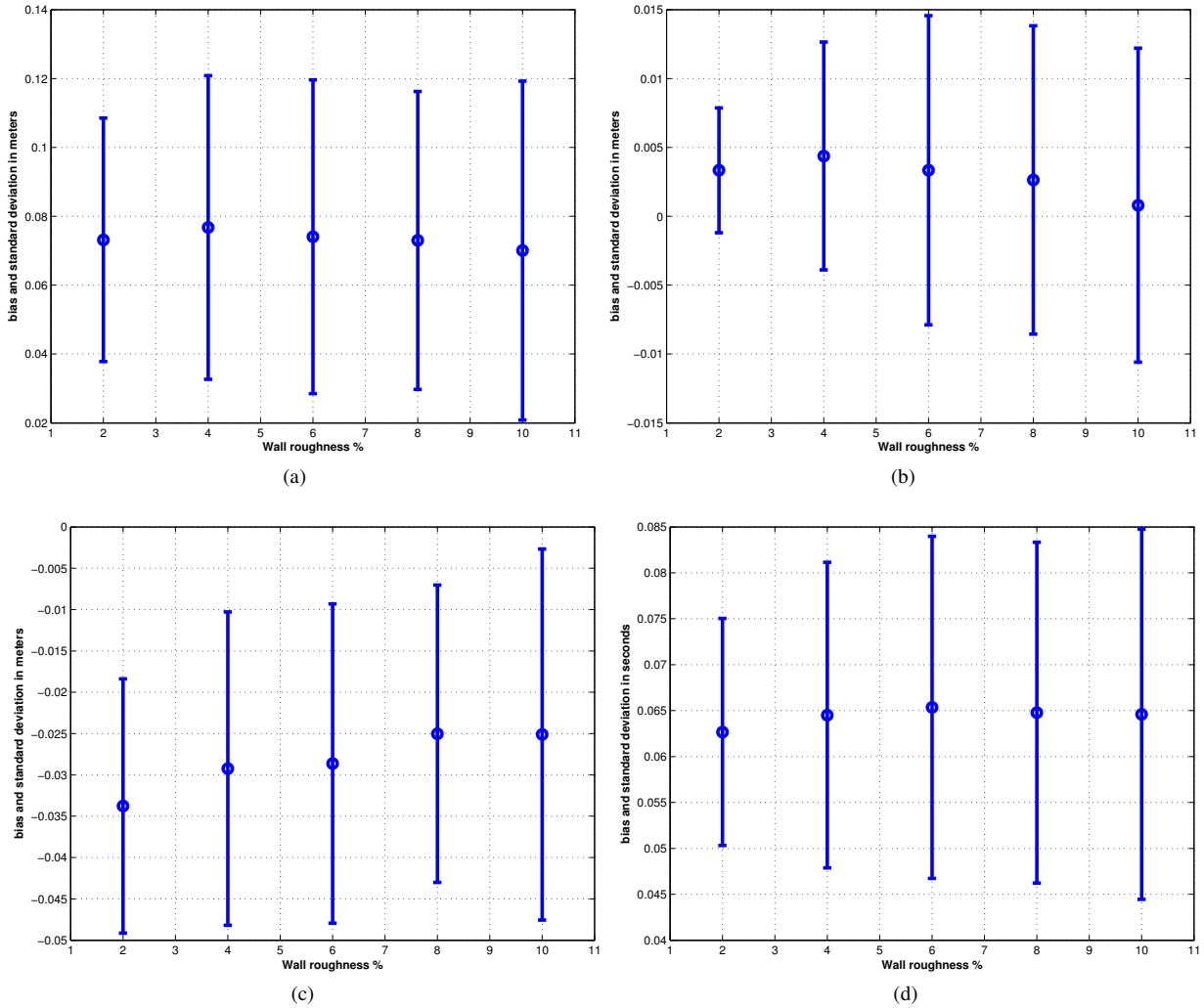

Fig. 9: Error bars (bias & standard deviation) of estimates: (a) x, (b) y, (c) z, (d) b, the time of emission, assuming correct association of the emitter. Results are shown for 100 Monte Carlo trials. The standard deviation of the wall roughness was varied from 2%-10% of the carrier wavelength, in increments of 2%. The weight parameter $\gamma = 0.6$.

TABLE III: Bias and standard deviation in estimated emitter position and time of emission, for a wall roughness of 3% the carrier wavelength, for varying (a) weight parameter γ, and (b) spatial correlation η of the sub-reflectors. Dimensions are in meters; the scene of interest has a size on the order of 10s of meters.

(a) $\eta = 0.3$

	$\gamma = 0.3$	$\gamma = 0.6$	$\gamma = 0.9$
Bias in estimated $[x, y, z, b]$	[0.2575,0.003, -0.1794,0.0522]	[0.0821,0.0031, -0.0327,-0.0673]	[0.0557,-0.0071, -0.0042,-0.0815]
Standard deviation in estimated $[x, y, z, b]$	[0.099, 0.0949, 0.0510, 0.0316]	[0.0436, 0.0316, 0.02, 0.02]	[0.0255, 0.0073, 0.0126, 0.0126]

(b) $\gamma = 0.6$

	$\eta = 0.3$	$\eta = 0.6$	$\eta = 0.9$
Bias in estimated$[x, y, z, b]$	[0.0826,0.0037, -0.0319,0.0678]	[0.0776,0.0031, -0.0309,0.0651]	[0.0780,0.0031, -0.0322,0.0652]
Standard deviation in estimated $[x, y, z, b]$	[0.048, 0.01, 0.0224, 0.0224]	[0.04,0.01, 0.0173,0.0173]	[0.0436,0.01, 0.02,0.02]

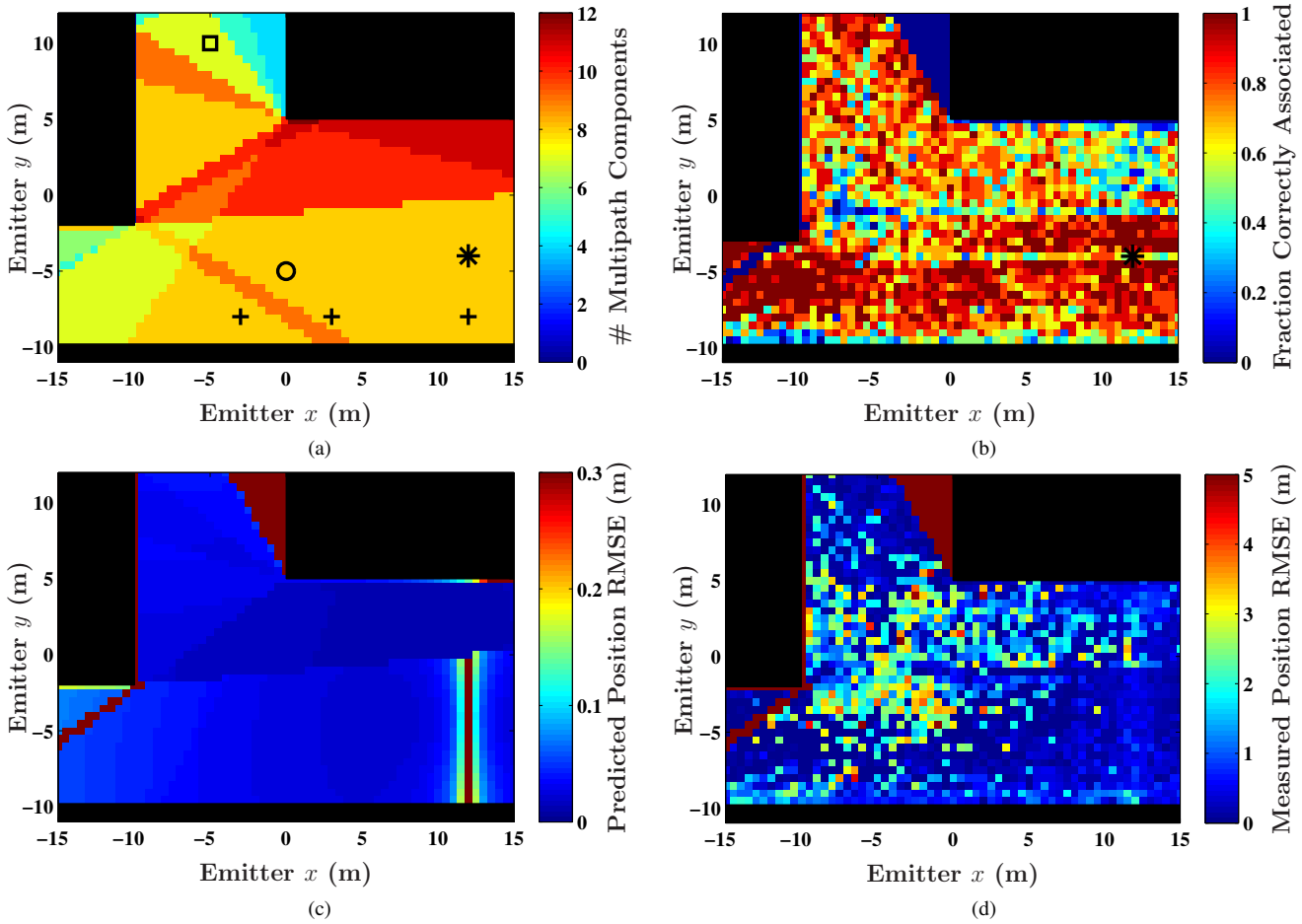

Fig. 10: In all images, the independent variables are the (x, y) components of the emitter position. The receiver is located at $\mathbf{r}_0 = (12, -4, 5)$, the point indicated by $*$. Clutter scatterers are at the points marked **+**. (a) shows the number of propagation paths for each emitter position. The square indicates an emitter position with no line-of-sight to the receiver, for which localization is nonetheless possible based on the 7 NLOS paths. (b) shows the fraction of trials in which the correct association was obtained. (c) shows the RMSE positioning error predicted by a first order analysis of the virtual receiver positions. (d) shows the RMSE positioning error actually achieved.

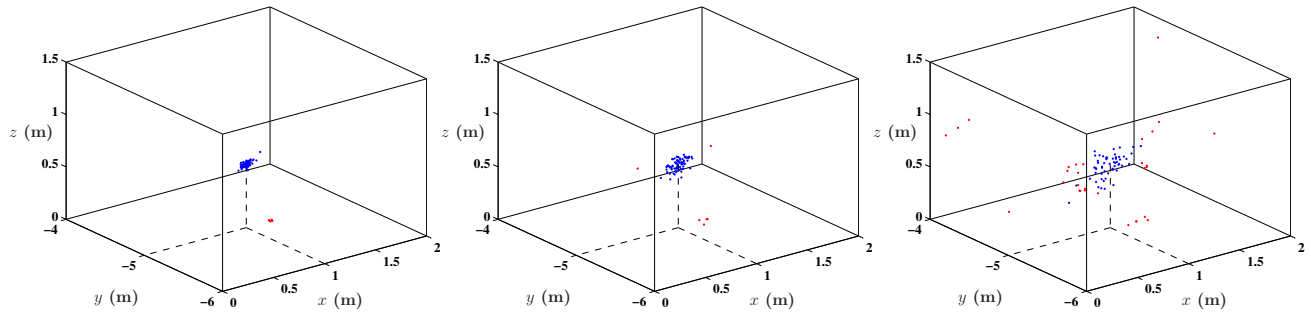

(a) $\sigma = 0.005/c$ (b) $\sigma = 0.01/c$ (c) $\sigma = 0.02/c$

Fig. 11: The estimated emitter position for 100 trials with clutter and noise with standard deviations $\sigma = \{0.005/c,\ 0.01/c,\ 0.02/c\}$. Blue points indicate position estimates for trials where the correct association is determined and clutter is rejected. At the lowest noise level (a), these are tightly clustered around the true emitter position, $\mathbf{e} = (1, -5, 0.6)$. The estimated positions in trials with erroneous associations are indicated by red points.

run with the range of TOA measurement uncertainties used in the first experiment, and with clutter as before. For this configuration, the number of measured TOAs was $M = 8$. Requiring varying number of associations, $K = 5, 6, 7, 8$, resulted in varying robustness to error, as shown in Figure 12. Requiring candidate solutions to make a larger number of associations greatly reduces the probability that solutions that erroneously associate clutter TOAs will be accepted.

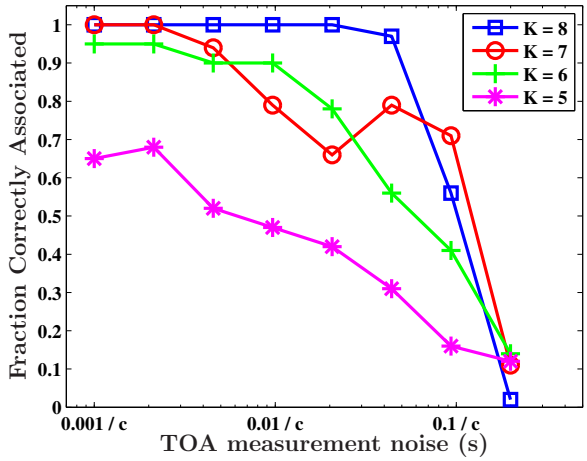

Fig. 12: This shows the fraction of correct association achieved for the emitter at $\mathbf{e} = (1, -5, 0.6)$ and receiver at $\mathbf{r_0} = (12, -4, 5)$. Setting $K = 8$ requires the algorithm to consider only candidate solutions with 8 or more associations and resulted in a higher fraction of trials with correct association than when K was set lower.

VI. Conclusion

This report described a method for localizing an emitter using only a single receiver by exploiting multipath scattering in a known environment. In contrast with past studies of multipath-based localization, we do not assume that the emitter and receiver are synchronized, and for this reason, the problem under consideration is one of pseudoranging, rather than ranging. The multipath TOA RF emitter localization problem can be made exactly equivalent to the GPS problem, by properly identifying the times of arrival of the multipath components with GPS pseudoranges, and the difference between the time of emission and time of arrival of the line-of-sight signal with the clock offset between the satellites and GPS receiver. Localization was based on the Bancroft method, an algebraic, weighted-least-squares solution to the GPS equations.

The main difficulty of the proposed approach was found to lie in correctly associating measured times-of-arrival of multipath components to known scattering surfaces. We described a test based on error residuals that can discriminate the correct association from erroneous associations. This same test is also useful for rejecting clutter returns. We also described an approximate solution method to the association problem that avoids combinatorial complexity at the cost of a small probability of missing the correct association. Finally, we analyzed in detail the performance of the localization method in the urban canyon geometry. The concept of geometric dilution of precision was used to determine the optimal receiver position.

The sensitivity of the proposed method to noise, clutter, and wall roughness were studied in Monte Carlo simulations. At high SNRs, the proposed solution to the association problem consistently selected the correct association and rejected clutter TOAs. It was seen via numerical modeling that roughness of the scattering surfaces causes a persistent, but small bias in the estimate of the emitter position. In all, we find that although single-sensor localization presents significant challenges, multipath exploitation could provide accurate localization of RF emitters for an interesting range of applications where coordination and synchronization of spatially-distributed receivers is not possible.

References

[1] A. Amar and A. J. Weiss. Localization of narrowband radio emitters based on Doppler frequency shifts. *IEEE Trans Sig Proc*, 56, 2008.

[2] S. Bancroft. An algebraic solution of the GPS equations. *IEEE Trans Aerosp Electron Syst*, 21:56–59, 1985.

[3] E. Baranoski. VisiBuilding: sensing through walls. In *IEEE Workshop Sensor Array and Multichannel Proc*, pages 1–22, 2006.

[4] K. Becker. An efficient method of passive emitter location. *IEEE Trans Aerosp Electron Syst*, 28(4):1091–1104, 1992.

[5] K. Becker. Passive localization of frequency-agile radars from angle and frequency measurements. *IEEE Trans Aerosp Electron Syst*, 35(4):1129–1144, 1999.

[6] Y. Chan, W.-Y. Tsui, H.-C. So, and P.-C. Ching. Time-of-arrival based localization under NLOS conditions. *IEEE Trans Vehicular Technology*, 55(1):17–24, 2006.

[7] P. C. Chen. A non-line-of-sight error mitigation algorithm in location estimation. In *IEEE Wireless Comm Networking Conf*, 1999.

[8] P. Chestnut. Emitter location accuracy using TDOA and differential Doppler. *IEEE Trans Aerosp Electron Syst*, 18(2):214–218, 1982.

[9] D. Dardari, A. Conti, U. Ferner, A. Giorgetti, and M. Z. Win. Ranging with ultrawide bandwidth signals in multipath environments. *Proc IEEE*, 97(2):404–426, 2009.

[10] J. Do, M. Rabinowitz, and P. Enge. Linear time-of-arrival estimation in a multipath environment by inverse correlation method. In *Proc Inst Navigation*, 2005.

[11] M. Gavish and A. J. Weiss. Performance analysis of bearing-only target location algorithms. *IEEE Trans Aerosp Electron Syst*, 28:817–828, 1992.

[12] G. Groves, J. Conte, and W. Blair. Preliminary analysis of the vertical-motion detection for low-elevation targets with Doppler processing at W-band. *Naval Surface Warfare Center Tech Report*, TR-94/351, 1994.

[13] D. E. Gustafson, J. M. Elwell, and J. A. Soltz. Innovative indoor geolocation using RF multipath diversity. In *IEEE Position Location and Navigation Symp*, 2006.

[14] K. Ho, X. Lu, and L. Kovavisaruch. Source localization using TDOA and FDOA measurements in the presence of receiver location errors: analysis and solution. *IEEE Trans Sig Proc*, 55(2):684–696, 2007.

[15] K. C. Ho and W. Xu. An accurate algebraic solution for moving source location using TDOA and FDOA measurements. *IEEE Trans Sig Proc*, 52:2453–2463, 2004.

[16] Z. Kostiç, M. I. Sezan, and E. L. Titlebaum. Estimation of the parameters of a multipath channel using set-theoretic deconvolution. *IEEE Trans Comm*, 40(6), 1992.

[17] J. Krolik, J. Farell, and A. Steinhardt. Exploiting multipath propagation for GMTI in urban environments. In *Proc IEEE Radar Conf*, 2006.

[18] X. Li and K. Pahlavan. Super-resolution ToA estimation with diversity for indoor geolocation. *IEEE Trans Wireless Comm*, 3(1):224–234, 2004.

[19] R. Linnehan and J. Schindler. Multistatic scattering from moving targets in multipath environments. In *IEEE Radar Conf*, 2009.

[20] K. Lui and H. So. Range-based source localisation with pure reflector in presence of multipath propagation. *Electronics Letters*, 46(13), 2010.

[21] P. Meissner and K. Witrisal. Multipath-assisted single-anchor indoor localization in an office environment. In *International Conf Systems, Signals and Image Processing*, pages 22–25, 2012.

[22] S. O. Rice. Reflection of electromagnetic waves from slightly rough surfaces. *Comm Pure and Appl Math*, 4(2-3):351–378, 1951.

[23] C. K. Seow and S. Y. Tan. Localization of omni-directional mobile device in multipath environments. *Progress in Electromagnetic Research*, 85:323–348, 2008.

[24] P. Setlur. *Statistical algorithms and bounds for moving targets in urban sensing and through-the-wall radar applications*. PhD thesis, Villanova University, 2010.

[25] P. Setlur, G. E. Smith, F. Ahmad, and M. G. Amin. Target localization with a single sensor via multipath exploitation. *IEEE Trans Aerosp Electron Syst*, 48(3):1996–2014, 2012.

[26] N. Shashidhar and G. Anand. Eigenray tracing in an ocean using Fermat's principle. *J Sound and Vibration*, 186(2):231 – 243, 1995.

[27] Y. Shen and M. Z. Win. On the use of multipath geometry for wideband cooperative localization. In *Proc IEEE Global Telecom Conf*, 2009.

[28] Y. Shen and M. Z. Win. Fundamental limits of wideband localization, part I: a general framework. *IEEE Trans Info Theory*, 56(10):4956–4980, 2010.

[29] S. Stein. Differential delay/Doppler ML estimation with unknown signals. *IEEE Trans Sig Proc*, 41:2717–2719, 1993.

[30] G. Strang. *Introduction to Linear Algebra*. Wellesley-Cambridge Press, 2003.

[31] A. Tabatabaeenejad and M. Moghaddam. Bistatic scattering from three-dimensional layered rough surfaces. *IEEE Trans Geoscience and Remote Sensing*, 44(8):2102 –2114, 2006.

[32] E. I. Thorsos. The validity of the Kirchhoff approximation for rough surface scattering using a Gaussian roughness spectrum. *J Acoustical Society of America*, 83(1):78–92, 1988.

[33] D. J. Torrieri. Statistical theory of passive location systems. *IEEE Trans Aerosp Electron Syst*, 20:183–198, 1984.

[34] C. Tsakostas. Image receiver model: An efficient variation of the image source model. In *Proc HELINA Conf*, 2004.

[35] M. Z. Win and R. Scholtz. Impulse radio: how it works. *IEEE Comm Letters*, 2(1):10–12, 1998.

[36] L. Yang and G. Giannakis. Ultra-wideband communications: an idea whose time has come. *IEEE Sig Proc Mag*, 21(6):26–54, 2004.